

# Modelling segregation effects of heterogeneous emissions on ozone levels in idealised urban street canyons: Using photochemical box models

Zhong, Jian; Cai, Xiaoming; Bloss, William

DOI:

[10.1016/j.envpol.2014.02.001](https://doi.org/10.1016/j.envpol.2014.02.001)

License:

None: All rights reserved

*Document Version*

Early version, also known as pre-print

*Citation for published version (Harvard):*

Zhong, J, Cai, X & Bloss, W 2014, 'Modelling segregation effects of heterogeneous emissions on ozone levels in idealised urban street canyons: Using photochemical box models', *Environmental Pollution*, vol. 188, pp. 132-143. <https://doi.org/10.1016/j.envpol.2014.02.001>

[Link to publication on Research at Birmingham portal](#)

## **Publisher Rights Statement:**

NOTICE: this is the author's version of a work that was accepted for publication in *Environmental Pollution*. Changes resulting from the publishing process, such as peer review, editing, corrections, structural formatting, and other quality control mechanisms may not be reflected in this document. Changes may have been made to this work since it was submitted for publication. A definitive version was subsequently published in *Environmental Pollution* Volume 188, May 2014, Pages 132–143. DOI: 10.1016/j.envpol.2014.02.001

## **General rights**

Unless a licence is specified above, all rights (including copyright and moral rights) in this document are retained by the authors and/or the copyright holders. The express permission of the copyright holder must be obtained for any use of this material other than for purposes permitted by law.

- Users may freely distribute the URL that is used to identify this publication.
- Users may download and/or print one copy of the publication from the University of Birmingham research portal for the purpose of private study or non-commercial research.
- User may use extracts from the document in line with the concept of 'fair dealing' under the Copyright, Designs and Patents Act 1988 (?)
- Users may not further distribute the material nor use it for the purposes of commercial gain.

Where a licence is displayed above, please note the terms and conditions of the licence govern your use of this document.

When citing, please reference the published version.

## **Take down policy**

While the University of Birmingham exercises care and attention in making items available there are rare occasions when an item has been uploaded in error or has been deemed to be commercially or otherwise sensitive.

If you believe that this is the case for this document, please contact [UBIRA@lists.bham.ac.uk](mailto:UBIRA@lists.bham.ac.uk) providing details and we will remove access to the work immediately and investigate.

# Modelling segregation effects of heterogeneous emissions on ozone levels in idealised urban street canyons: using photochemical box models

Jian Zhong, Xiao-Ming Cai<sup>\*</sup> and William James Bloss

School of Geography, Earth & Environmental Sciences, University of Birmingham, Edgbaston, Birmingham, B15 2TT, UK

<sup>\*</sup> Corresponding author. Tel.: (0121) 4145533; Fax: (0121) 4145528.

Email address: [x.cai@bham.ac.uk](mailto:x.cai@bham.ac.uk) (X.-M. Cai).

## Abstract

Air quality models include representations of pollutant emissions, which necessarily entail spatial averaging to reflect the model grid size; such averaging may result in significant uncertainties and/or systematic biases in the model output. This study investigates such uncertainties, considering ozone concentrations in idealised street canyons within the urban canopy. A photochemical model with grid-averaged emissions of street canyons is compared with a multiple-box model considering each canyon independently. The results reveal that the averaged, ‘one-box’ model may significantly underestimate true (independent canyon mean) ozone concentrations for typical urban areas, and that the performance of the averaged model is improved for more ‘green’ and/or less trafficked areas. Our findings also suggest that the trends of 2005-2020 in emissions, in isolation, reduce the error inherent in the averaged-emissions treatment. These new findings may be used to evaluate uncertainties in modelled urban ozone concentrations when grid-averaged emissions are adopted.

## Capsule:

A grid-based urban air quality model, if adopting a grid-averaging scheme of emissions from segregated street canyons, may significantly underestimate the street-level ozone abundance.

**Keywords:** Segregation effect; urban street canyon; emission heterogeneity; photochemical box model; urban ozone concentrations.

## Nomenclature

$C_{i,m}$	: Concentration of $i^{\text{th}}$ species in Box $m$ ( $m=0,1,2$ ) (ppb);
$C_{bi,m}$	: Background concentration of $i^{\text{th}}$ species for Box $m$ ( $m=0,1,2$ ) (ppb);
$C_{i,1+2}$	: Averaged concentration of Boxes 1 and 2 of the $i^{\text{th}}$ species (ppb);
$E_{i,m}$	: Emission rate of the $i^{\text{th}}$ species in Box $m$ ( $m=0,1,2$ ) (ppb $\text{s}^{-1}$ );
$H_m$	: Height of the street canyon of Box $m$ ( $m=0,1,2$ ) (metre);
$I_{S(A+B)}$	: Intensity of segregation between species A and B;
$k_{(A+B)}$	: Second-order rate constant for species A and B in a well-mixed box;
$\langle k_{\text{eff}(A+B)} \rangle$	: Effective second-order rate constant in the ‘two-box’ model;
RSL	: Region Split Line;
$t$	: Time (s);
$w_{i,m}$	: Exchange velocity between street canyon and background for Box $m$ ( $m=0,1,2$ ) ( $\text{m s}^{-1}$ );
$\Delta S_{i,m}$	: Net chemical production rate of the $i^{\text{th}}$ species in Box $m$ ( $m=0,1,2$ ) (ppb $\text{s}^{-1}$ );
$\varepsilon$	: Heterogeneity of emissions;
$\phi_i$	: Percentage of overestimation for the $i^{\text{th}}$ species by the ‘one-box’ model (%);

28

## 29 1 Introduction

30 Atmospheric chemical and physical processes are tightly coupled in air quality simulations  
31 (Karamchandani et al., 2012). A general operating hypothesis of most urban air quality grid-  
32 based models is that primary air pollutants emitted from vehicles, industry or other sources  
33 are instantaneously well-mixed or distributed within the entire model grid-cell which contains  
34 the emissions (Auger and Legras, 2007). The grid-averaged emission rates of primary air  
35 pollutants are normally used as an input representing the mean gridded emissions (Denby et  
36 al., 2011) in atmospheric chemical models and the concentration in the canopy layer is  
37 modelled as one box representing the canopy layer for the entire grid cell. However, in reality  
38 these surface emissions vary, and exhibit a high temporal and spatial heterogeneous  
39 distribution at the sub-grid scale, referred to as surface sub-grid emission heterogeneity  
40 (Galmarini et al., 2008). This leads to segregation effects due to incomplete mixing. In the  
41 grid-averaging procedure, all sub-grid scale processes and features (Ching et al., 2006) are

lost and secondary pollutants (e.g. O<sub>3</sub>) may therefore be systematically under- or over-estimated.

Several model approaches have been suggested to account for the impacts of sub-grid emission heterogeneity. Nested-grid or high-resolution modelling is a simple approach to resolve sub-grid scale variability. Examples of such approach can be seen from the Community Multiscale Air Quality (CMAQ) model (Sokhi et al., 2006; Shrestha et al., 2009), the Weather Research and Forecasting/Chemistry (WRF/Chem) model (Grell et al., 2005), and the Comprehensive Air Quality Model with extensions (CAMx) (Shen et al., 2011). A shortage of this approach is that it is only effective locally to a fixed area where the finer resolution grid is located. In order to overcome the limitation, adaptive grid modelling (Srivastava et al., 2000; Constantinescu et al., 2008; Garcia-Menendez et al., 2010) was developed to allow dynamic change of the grid system during a simulation. Garcia-Menendez and Odman (2011) discussed the details and reviewed the advances of the adaptive grid modeling. Another approach to incorporate sub-grid emission heterogeneity is hybrid modeling, which combines a regional grid-based model with a local Gaussian dispersion model (e.g. ADMS (Arciszewska and McClatchey, 2001) and AERMOD (Zou et al., 2010)). This approach has been extensively implemented, such as the CMAQ-ADMS model (Chemel et al., 2011; Beevers et al., 2012; Stocker et al., 2012), the CMAQ-AERMOD model (Stein et al., 2007; Isakov et al., 2009; Johnson et al., 2010) and the WRF-AERMOD model (Kesarkar et al., 2007). A more promising approach is the plume-in-grid (PinG) modelling (Karamchandani et al., 2002), which imbeds a non-steady-state plume model inside the grid. Vijayaraghavan et al. (2006) implemented the plume-in-grid (PinG) modelling approach in the CMAQ-APT model to reduce sub-grid scale variability in a simulation of central California. They found that the sub-grid treatment can lead to up to 10 ppb less O<sub>3</sub> under the condition of O<sub>3</sub> formation and up to 6 ppb more O<sub>3</sub> under other conditions, compared with a base simulation without the PinG treatment. The approach offers a more realistic representation of the elevated point emission sources and their atmospheric fate. Galmarini et al. (2008) developed a Reynolds-average model to parameterize sub-grid emission heterogeneity in the meso- and global scale. Their study built upon the assumption that concentrations can be divided into a mean part, depending upon the average emissions, and a fluctuation component which depends on the variability of emissions, respectively. Alternatively, Cassiani et al. (2010) developed a stochastic fields method to address surface sub-grid emission heterogeneity in a mesoscale dispersion model. The advantage of this

method is that the sub-grid scale emission variability is well-represented by the probability density functions. Some of the above approaches to address sub-grid scale errors are also reviewed and discussed in details by Touma et al. (2006) and Karamchandani et al. (2011). Currently, strategies to address sub-grid emission heterogeneity are mostly focussed upon large scale grid-based models. However, for the small scale, there is little research focusing on the effects of sub-grid emission heterogeneity.

Here, we extend consideration of emissions heterogeneity to the small scale, i.e. the canyon scale. The canopy layer is a major source for emissions into the overlying atmosphere / boundary layer and is normally within the lowest grid-cell of a grid-based model. From the canopy layer perspective, urban street canyons are typical sub-grid scale features separated by rows of buildings. These emissions into the canyon layer may be pre-processed within urban street canyons before they enter to the entire grid-cell in the lowest part of the grid-based model (Fisher et al., 2006). Urban street canyons, where human exposure takes place, are the area of interest in this paper. The additional information between the grid-averaging implementation and the sub-grid calculation taking the emission heterogeneity into consideration may be of importance in terms of accurately calculating air pollutant abundance and their associated adverse health effects.

The aim of this study is to investigate segregation effects of heterogeneous emissions on  $O_3$  levels in idealised urban street canyons, and to identify how segregation effects are influenced by the balance between chemistry and dynamics. The paper is structured as follows. In Section 2, the methodology based on photochemical box models is described in details, as well as the corresponding concept of intensity of segregation and the model scenarios. In the following sections, the results for prediction of ozone levels and the intensity of segregation are discussed.

## **2 Methodology**

There are a large number of possible arrangements of street canyons in the urban canopy layer. In this study, we select two typical idealised urban street canyons as a representation. One large photochemical box model (hereafter referred to as the ‘one-box’ model) with averaged emissions of the two street canyons is used to represent the deterministic calculation based on the grid-average process; alternatively two small photochemical boxes (hereafter referred to as the ‘two-box’ model) are combined to represent two segregated street canyons with their own respective emissions. The photochemical box models (which assume that

chemical species inside each box are well-mixed) can be simply applied and computationally inexpensive simulated. The model is written in FORTRAN77 language and run using FACSIMILE 4 integrator (Curtis and Sweetenham, 1987). A reduced chemical scheme (RCS), developed by Bright et al. (2013), is used as the chemical mechanism within the photochemical box models. The detailed model configuration is described as follows.

## 2.1 Model Setup

Figure 1 illustrates the overview of the box model configuration. It is assumed that in a cell of an urban air quality model, there are two street canyons with heterogeneous emissions represented by Box 1 and Box 2 with the same volume of air as indicated in the right panel (i.e. ‘Two-box model’) of Figure 1. There is no exchange between the two boxes, i.e. total segregation is assumed; we only consider exchange between the within-canyon air and the background air above the canopy layer. It is also assumed that the ‘two-box’ model represents the reality and the mean concentration,

$$C_{i,1+2} = (C_{i,1} + C_{i,2}) / 2 \quad (1)$$

represents the ‘true’ concentration of the  $i^{\text{th}}$  species in the canopy layer corresponding to this cell, with the concentrations in the ‘one-box’ model departing from this truth due to segregation effects. If a simplified approach of one single box (Box 0 indicated in the left panel of Figure 1) is adopted in which the volume of Box 0 is the sum of the volumes of Box 1 and Box 2 (indicated in the right panel of Figure 1) and  $C_{i,0}$  is the modelled concentration from the ‘one-box’ model (Box 0 in Figure 1), there would be an error for  $C_{i,0}$  (either an overestimation or an underestimation) in comparison with the ‘true’ mean concentration  $C_{i,1+2}$  derived from the ‘two-box’ model (Box 1 and Box 2 in Figure 1). This error is expressed as

$$\Delta C_i = C_{i,0} - C_{i,1+2} \quad (2)$$

We may also interpret  $\Delta C_i$  as the concentration difference due to heterogeneity of emissions, or the overestimated concentration by Box 0. For individual reactive species in the ‘one-box’ model (Box 0), the mass transport can be described as the following equation (Liu and Leung, 2008):

$$\frac{d}{dt} C_{i,0}(t) = E_{i,0} - \frac{w_{t,0}}{H_0} (C_{i,0} - C_{bi,0}) + \Delta S_{i,0} \quad (3)$$

Where,  $C_{i,0}$  (ppb) is the concentration of  $i^{\text{th}}$  species by volume in Box 0,  $t$  (s) is the time,  $E_{i,0}$  (ppb  $\text{s}^{-1}$ ) is the emission rate of  $i^{\text{th}}$  species by volume in Box 0,  $w_{t,0}$  ( $\text{m s}^{-1}$ ) is the exchange velocity between the street canyon and background for Box 0,  $H_0$  (m) is the height of the street canyon of Box 0,  $C_{bi,0}$  (ppb) is the background concentration of  $i^{\text{th}}$  species of Box 0 and  $\Delta S_{i,0}$  (ppb  $\text{s}^{-1}$ ) is the net production rate of  $i^{\text{th}}$  species due to chemical reactions in Box 0. Similarly, the system of equations in the ‘two-box’ model (Box 1 and Box 2) can be expressed as follows:

$$\frac{d}{dt} C_{i,1}(t) = E_{i,1} - \frac{w_{t,1}}{H_1} (C_{i,1} - C_{bi,1}) + \Delta S_{i,1} \quad (4)$$

$$\frac{d}{dt} C_{i,2}(t) = E_{i,2} - \frac{w_{t,2}}{H_2} (C_{i,2} - C_{bi,2}) + \Delta S_{i,2} \quad (5)$$

In Equations (4) and (5), all symbols are as those in Equation (3) but for Box 1 and Box 2, respectively. In our model, we assume that  $w_{t,0} = w_{t,1} = w_{t,2}$ ,  $C_{bt,0} = C_{bt,1} = C_{bt,2}$ ,  $E_{i,1} = E_{i,0}(1 + \varepsilon)$  and  $E_{i,2} = E_{i,0}(1 - \varepsilon)$ , where  $\varepsilon$  is the heterogeneity of emissions for the two-box model (e.g.  $\varepsilon = 0$ : homogeneous emissions for the two boxes;  $\varepsilon = 1$ : all emissions into Box 1 and no emissions into Box 2). When the systems reach the steady state (or a quasi-steady state) as  $t \rightarrow t_s$ , then  $\frac{d}{dt} C_{i,m}(t) \rightarrow 0$  ( $m=0,1,2$ ), and Equations (3)-(5) yield:

$$C_{i,0}(t_s) = \frac{H_0}{w_{t,0}} [E_{i,0} + \Delta S_{i,0}(t_s)] + C_{bi,0} \quad (6)$$

$$C_{i,1}(t_s) = \frac{H_1}{w_{t,1}} [E_{i,1} + \Delta S_{i,1}(t_s)] + C_{bi,1} \quad (7)$$

$$C_{i,2}(t_s) = \frac{H_2}{w_{t,2}} [E_{i,2} + \Delta S_{i,2}(t_s)] + C_{bi,2} \quad (8)$$

$$C_{i,1+2}(t_s) = [C_{i,1}(t_s) + C_{i,2}(t_s)] / 2 \quad (9)$$

Thus the concentrations  $C_{i,m}$  and the chemical production rate  $\Delta S_{i,m}$ , for  $m=0,1,2$ , are related by above respective equations. The relationships are a function of the corresponding emission rates and background conditions, respectively. It is noted that, from (2), (6)-(9), we have

$$\Delta C_i(t_s) = \frac{H_0}{w_{i,0}} [\Delta S_{i,0}(t_s) - \frac{\Delta S_{i,1}(t_s) + \Delta S_{i,2}(t_s)}{2}] \quad (10)$$

If the emission is a passive scalar (i.e. a species which does not undergo chemical reaction), then the difference  $\Delta C_i(t_s)$  is zero. For reactive species, the differences depend on the heterogeneity of emissions and the nonlinear nature of photochemical reactions, together with the exchange velocity caused by dynamic effects. Therefore the characteristics of  $\Delta C_i(t_s)$  can be complex and will be examined in depth in the following sections.

Finally, we define the *percentage of overestimation* by the ‘one-box’ model (Box 0) for the  $i^{\text{th}}$  species as:

$$\phi_i(t) = \frac{\Delta C_i(t)}{C_{i,1+2}(t)} \times 100\% \quad (11)$$

$\phi_i(t)$  may also be interpreted as the overestimated concentration by the ‘one-box’ model relative to the ‘true’ concentration by the ‘two-box’ model. If  $\phi_i(t) = 0\%$ , it means that the ‘one-box’ model provides the true answer; if  $\phi_i(t) = 10\%$  or  $-10\%$ , it means that Box 0 over- or under-estimates the concentration by 10%, respectively.

## 2.2 Intensity of segregation

In order to characterise the sub-grid scale variability due to incomplete mixing, a widely used dimensionless number, the *intensity of segregation* (Krol et al., 2000) between two chemical species A and B,  $I_{S(A+B)}$ , is introduced and defined as

$$I_{S(A+B)} = \frac{\langle A'B' \rangle}{\langle A \rangle \langle B \rangle} \quad (12)$$

where the angle brackets represent the volume average, the prime denotes the local deviation from the volume-averaged concentration, and  $A'B'$  stands for the covariance between A and B. For any species A in the ‘two-box’ model of this study,  $\langle A \rangle = \frac{1}{2}(A_1 + A_2)$  is A’s mean concentration of the two boxes,  $A_1$  and  $A_2$  are A’s concentrations in Box 1 and Box 2, respectively,  $A'_1 = A_1 - \langle A \rangle$ ,  $A'_2 = A_2 - \langle A \rangle$  and  $\langle A'B' \rangle = \frac{1}{2}(A'_1 B'_1 + A'_2 B'_2)$ . The intensity of



segregation between A and B is a proper measure of the effect of segregation on nonlinear chemical processes (Hilst, 1998). For a second-order reaction  $A+B \rightarrow C$  in a heterogeneously system (i.e. the ‘two-box’ model in this study), the formation of C (Vinuesa and de Arellano, 2005) can be described as follows,

$$\frac{d\langle C \rangle}{dt} = \langle k_{eff(A+B)} \rangle \langle A \rangle \langle B \rangle \quad (13)$$

where  $\langle k_{eff(A+B)} \rangle$  is the effective second-order rate constant for formation of C in the ‘two-box’ model which can be represented by

$$\langle k_{eff(A+B)} \rangle = k_{(A+B)} (1 + I_{S(A+B)}) \quad (14)$$

where  $k_{(A+B)}$  is the original rate constant of the reaction in the well-mixed ‘one-box’ model. Such a constant is normally obtained from laboratory experiments in a well-mixed chamber.

If  $I_{S(A+B)} = 0$ , it means that species A and B can be regarded as well-mixed; If  $I_{S(A+B)} > 0$  or  $I_{S(A+B)} < 0$ , it implies that  $\langle k_{eff(A+B)} \rangle$  in the ‘two-box’ model is larger or smaller than  $k_{(A+B)}$  in the ‘one-box’ model due to the effect of segregation.

## 2.3 Model Scenarios

### 2.3.1 Initial and background conditions

The initial conditions of the box models in this study were taken from those used in Bright et al. (2013) which in turn were based upon atmospheric field data from the Tropospheric Organic CHEmistry (TORCH) experiment (Lee et al., 2006). The photochemical box model is run without emissions for the first 30 minutes in order to spin up the model, which allows concentrations of intermediate species to be calculated. Then the concentrations of all species at 30 min are used as the background conditions in the boundary layer for exchange with the inside canyon environment for all the simulations.

### 2.3.2 Emissions and case settings

Drawing upon the UK Road Vehicle Emission Factors (Boulter et al., 2009), emission rates for  $NO_x$ , VOCs and CO of 620, 128 and 1356 g km<sup>-1</sup> hr<sup>-1</sup> were used respectively, which represent an urban continuous road traffic of 1500 vehicles hr<sup>-1</sup> with an average speed of 30

mph for the year of 2010 (Bright et al., 2013). The emission rates into a volume of urban street canyons ( $18\text{ m} \times 18\text{ m} \times 1\text{ m}$ ) are equivalent to  $E_{NO_x}=0.28$ ,  $E_{VOCs}=0.22$  and  $E_{CO}=1.0\text{ ppb s}^{-1}$  (here referred to a ‘Typical Real-world Emission Scenario’, TRES) for the  $NO_x$ , VOCs and CO, respectively. This canyon geometry was used by Bright et al. (2013) for their large-eddy simulations. In this study,  $E_{CO}$  is set as  $1.0\text{ ppb s}^{-1}$  for all the scenarios, and the representative  $E_{NO_x}$  and  $E_{VOCs}$  are scaled by different factors between 0.1 and 2 in order to characterize a wide range of real scenarios, i.e.  $E_{NO_x}$  varies from  $0.028$  to  $0.56\text{ ppb s}^{-1}$  in steps of  $0.028\text{ ppb s}^{-1}$ , while  $E_{VOCs}$  varies from  $0.022$  to  $0.44\text{ ppb s}^{-1}$  in steps of  $0.022\text{ ppb s}^{-1}$ . The ratio of primary NO to  $NO_2$  emission rate is 9:1, while the relative fractional VOCs emission rates are 44% for  $C_2H_4$ , 19% for  $C_3H_6$ , 25% for HCHO and 12% for  $CH_3CHO$  (as mixing ratio by volume) for all the scenarios.

In this study we focus on the effects of two parameters,  $\varepsilon$  (heterogeneity of emissions) and  $w_t$  (exchange velocity), on  $\phi_i$  and other characteristics. Table 1 gives an overview of the two parameters for all cases. For each case, the corresponding one photochemical box model (i.e. the ‘one-box’ model, Box 0) and two segregated photochemical box models (i.e. the ‘two-box’ model, Box 1 and Box 2) were run. The heterogeneity of emissions ( $\varepsilon$ ) is set at a value of 0.5 and the exchange velocity ( $w_t$ ) is set as  $0.02\text{ m s}^{-1}$  in the base case, ‘BASE’. The value of  $\varepsilon=0.5$  implies that the emissions into Box 1 (or Box 2) is 50% higher (or lower) than the averaged emissions parameterized into Box 0. In reality, this is often the case; within an Eulerian cell of an urban air quality model, some streets may have a much higher level of traffic than others. The value of  $w_t=0.02\text{ m s}^{-1}$  is adopted based on the result from a large-eddy simulation for a street canyon with a  $18\text{ m} \times 18\text{ m}$  cross-section under a neutral condition if the reference wind speed is about  $2\text{ m s}^{-1}$  (Cai, 2012).

In order to account for the segregation effect due to variations of  $\varepsilon$  and  $w_t$ , we examine in detail the cases in which  $\varepsilon$  and  $w_t$  are perturbed by 40%, respectively. Case HE-L and HE-H (see Table 1 for definitions) have been configured for 40% lower and higher  $\varepsilon$ , respectively, than 0.5, while keeping the same  $w_t$  as that of Case BASE. To consider the effect of exchange velocity ( $w_t$ ), we set up the cases of EX-L and EX-H for 40% lower and higher  $w_t$ , respectively, than  $0.02\text{ m s}^{-1}$ , while keeping the same  $\varepsilon$  as that of Case BASE. The range of values of  $w_t$  from  $0.012\text{ m s}^{-1}$  to  $0.028\text{ m s}^{-1}$  is justified based on previous findings that  $w_t$  varies when the canyon aspect ratio ( $H/W$ , where  $H$  is the building height and  $W$  is the street

width) is altered from 1 to a higher or lower value (e.g. Chung and Liu, 2013) and that urban surface heating may enhance  $w_t$  significantly (e.g. Cai, 2012).

### 3 Results and discussion

#### 3.1 Overestimation of ozone levels

Figure 2 depicts  $C_{O_3,1+2}$  (ppb), i.e. the ‘true’ concentration derived from the ‘two-box’ model, for all cases listed in Table 1 as a function of  $E_{NOx}$  and  $E_{VOCs}$ , once the simulations had reached a quasi-steady state (here defined as at  $t=4$  hr). The ranges of  $C_{O_3,1+2}$  for all cases are listed in Table 2, which reveals that the range of  $C_{O_3,1+2}$  strongly depends on the variation of  $w_t$  (indicated in Figure 2(d) and Figure 2(e)) rather than the variation of  $\varepsilon$  (indicated in Figure 2(b) and Figure 2(c)) and that the maximum range of  $C_{O_3,1+2}$  is (5.62, 160.82) ppb for Case EX-L with the lowest exchange velocity ( $0.12 \text{ m s}^{-1}$ ). In this study, the background  $O_3$  concentration is approximately 43.61 ppb and by using a Region Split Line (RSL) we divide the plot area into 2 regions, i.e. Region I (with the ratio of  $E_{VOCs}$  to  $E_{NOx}$  lower than the slope of RSL) for which  $C_{O_3,1+2}$  is lower than 43.61 ppb and Region II (with the ratio of  $E_{VOCs}$  to  $E_{NOx}$  higher than the slope of RSL) for which  $C_{O_3,1+2}$  is higher than 43.61 ppb. The RSL for all cases is marked in Figure 2. Figure 2(f) indicates that the RSL for Cases BASE, HE-H and HE-L exhibits the same slope with the  $E_{VOCs}:E_{NOx}$  ratio (by volume) of 2.6, and the slopes of the RSL are 1.9 for Cases EX-L and 3.4 for Cases EX-H (listed in Table 2). Therefore, we may conclude that the slope of the RSL depends on  $w_t$  but not on  $\varepsilon$ , and that the higher  $w_t$ , the higher the slope of the RSL. In Region I, the titration effect of  $O_3$  by NO is dominant and therefore leads to the net destruction of  $O_3$  (i.e. lower than the background levels). However, in Region II, OH oxidation processes are dominant and sufficient VOCs are present to promote the conversion of NO to  $NO_2$  by peroxy radicals, thereby causing net ozone formation. It is therefore not surprising that  $C_{O_3,1+2}$  is higher than its background level in Region II. The TRES (i.e.  $E_{NOx}=0.28 \text{ ppb s}^{-1}$ ,  $E_{VOCs}=0.22 \text{ ppb s}^{-1}$ ) defined in Section 2.3.2 is marked in the plots (triangle symbol); this emissions scenario, with the  $E_{VOCs}:E_{NOx}$  ratio (by volume) of 0.786, falls into Region I for all cases. This represents the typical situation in an urban area, namely that the ozone concentration inside a street canyon is lower than that in the overlying background atmosphere. It is noted in Figure 2(f) that the TRES is relatively closer to the RSL for Case EX-L, in which the exchange velocity between the canyon and the

boundary layer aloft,  $w_t$ , is 40% lower than the base case. A low  $w_t$  might be caused by a calm, stable meteorological condition or by a high canyon aspect ratio (i.e. large  $H/W$ ). The trajectory from 2005 to 2020 in Figure 2 represents the emission scenarios of these years, which are derived from the UK fleet composition projections (NAEI, 2003) and the UK Road Vehicle Emission Factors (Boulter et al., 2009) assuming constant traffic volume and speed same as the ‘TRES’ for 2010. Figure 2 shows that the trajectory from 2005 to 2020 falls into Region I and is approaching to the RSL with the reduction of VOCs and  $\text{NO}_x$  emissions due to current and future control technologies, assuming constant activity (i.e. traffic) levels.

Figure 3 illustrates the transects of  $C_{\text{O}_3,1+2}$  (ppb) through the emission scenarios in Figure 2(f). The rationale behind the choices is explained as follows. The dashed line, the dotted line and the dot-dash line all pass through the point for the TRES, as marked in Figure 2(f). The emission profile along this dashed line at the fixed  $E_{\text{NO}_x}$  of  $0.28 \text{ ppb s}^{-1}$  (Figure 3(a)) represents a technology of targeting only  $E_{\text{VOCs}}$  from vehicles, or the roads with a varying coverage of vegetation which may emit further VOCs into the urban canopy (Loughner et al., 2012). The emission profile along this dotted line at the fixed  $E_{\text{VOCs}}$  of  $0.22 \text{ ppb s}^{-1}$  (Figure 3(b)) represents a technology of targeting only  $E_{\text{NO}_x}$ . The emission profile along the dot-dash line (Figure 3(c)) represents a technology of both  $E_{\text{VOCs}}$  and  $E_{\text{NO}_x}$  (“TRES-2010”) with the proportional traffic-emitting rate of both VOCs and  $\text{NO}_x$  for the TRES. This dot-dashed line may also represent control of the number of vehicles in streets or scenarios for different areas (busier or less busy roads) with the same fleet composition as the TRES. The trajectory (Figure 3(d)) indicates emission scenarios for the years 2005 to 2020 with the same traffic volume and speed as the TRES. Figures 3(a) & 3(b) demonstrate that  $C_{\text{O}_3,1+2}$  increases with  $E_{\text{VOCs}}$  for the “Fixed  $E_{\text{NO}_x}$ ” scenario, but decreases with  $E_{\text{NO}_x}$  for the “Fixed  $E_{\text{VOCs}}$ ” scenario. Figure 3(c) suggests that for less busier roads than the TRES,  $C_{\text{O}_3,1+2}$  is higher, and vice versa. Figure 3(d) shows that as control technologies are applied,  $C_{\text{O}_3,1+2}$  increases. By 2020 it will be very close to the background level, particularly for Case EX-L for which the canopy layer is less ventilated. A higher ozone concentration also occurs to Case EX-L when  $E_{\text{VOCs}}$  is very high for the “Fixed  $E_{\text{NO}_x}$ ” scenario (Figure 3(a)) or when  $E_{\text{NO}_x}$  is very low for the “Fixed  $E_{\text{VOCs}}$ ” scenario (Figure 3(b)). The results show a nonlinear relationship between the  $\text{O}_3$  concentration and  $E_{\text{VOCs}}$  and/or  $E_{\text{NO}_x}$ , which is in line with many previous studies (e.g. Liu

and Leung, 2008). The TRES is indicated by a solid line in Figure 3(a)-(d) and  $C_{O_3,1+2}$  for all cases with the TRES are about 20 ppb with a small variation across those scenarios tested. However, the analysis below demonstrates that these concentrations by the ‘two-box’ model will be significantly underestimated by the ‘one-box’ model.

Figure 4 shows the values for  $\phi_{O_3}$  (the percentage of overestimation for  $O_3$  by the ‘one-box’ model) for all cases listed in Table 1 at  $t=4$  hr. It is interesting to notice that the RSL (defined above) of each case splits the plot area into two regions, i.e. Region I where  $\phi_{O_3}$  is negative and Region II where  $\phi_{O_3}$  is positive. In Region I,  $\phi_{O_3}$  is negative, which means the modelled  $O_3$  concentration by the ‘one-box’ model is lower than the ‘true’ value by the ‘two-box’ model (i.e. the ‘one-box’ model will underestimate  $O_3$  levels). It is further shown that if only  $\varepsilon$  is changed from 0.5 (Figure 4(a)) to 0.7 (Figure 4(c)) and to 0.3 (Figure 4(b)), respectively, a rapid change in  $\phi_{O_3}$  is found. The maximum underestimation could be up to -35.24 % for Case HE-H (Figure 4(c)), and the minimum underestimation could be -6.12 % for Case HE-L (Figure 4(b)). The larger  $\varepsilon$  is, the higher the maximum level of  $\phi_{O_3}$  will be. It is also noted that if only the exchange velocity ( $w_t$ ) is changed from 0.020  $m\ s^{-1}$  (Figure 4(a)) to 0.012  $m\ s^{-1}$  (Figure 4(d)) and to 0.028  $m\ s^{-1}$  (Figure 4(e)), respectively, there is a less significant change in the maximum level of  $\phi_{O_3}$  (listed in Table 2). However, there are noticeable shifts of the RSL (discussed above) and the isopleths patterns associated with the variation of  $w_t$ . The trajectory from 2005 to 2020 falls into the underestimation area (i.e. Region I), and is marked in the plot for each case. In Region II for all the cases, the  $O_3$  levels will be slightly overestimated up to 3.07 % obtained for Case HE-H (Table 2).

Figure 5 shows the transects of  $\phi_{O_3}$  through the lines in Figure 4(f). For the TRES emission scenario for the year of 2010 indicated by the solid line in Figure 5, underestimates of  $O_3$  concentration by the ‘one-box’ model are -12.37% for Case BASE, -4.31% for Case HE-L, -25.07% for Case HE-H, -8.90% for Case EX-L and -12.30% for Case EX-H, respectively, suggesting that the effect of emission heterogeneity is more significant than the effect of exchange velocity.

328

329 Figure 5(a) shows that as  $E_{VOCs}$  increases at the fixed  $E_{NOx}$  of 0.28 ppb s<sup>-1</sup>, the modelled O<sub>3</sub>  
330 concentrations by the ‘one-box’ model are underestimated compared with the ‘true’ values,  
331 indicated by the negative  $\phi_{O_3}$ . The lower  $E_{VOCs}$  is, the larger the extent of underestimation  
332 will be. Figure 5(a) also indicates that by keeping traffic-emission rate  $E_{NOx}$  unchanged, extra  
333  $E_{VOCs}$  (e.g. from vegetation or anthropogenic activities) will reduce  $\phi_{O_3}$ , resulting in the  
334 improved performance of the ‘one-box’ model. However, future reduction in vehicle-related  
335  $E_{VOCs}$ , anticipated to arise from renewal of the vehicle fleet and implementation of more  
336 stringent emissions reduction technologies, will lead to an increase in the magnitude of  $\phi_{O_3}$ .  
337 This also suggests that the performance of the ‘one-box’ model for O<sub>3</sub> concentration might be  
338 expected to be better for a more ‘green’ area, with biogenic VOC emissions, assuming such  
339 emissions were not incorporated in the model scenario / conditions.

340

341 Figure 5(b) illustrates the results of  $\phi_{O_3}$  along the dotted line of Figure 4(f), i.e. varying  $E_{NOx}$   
342 for a fixed  $E_{VOCs}$  corresponding to the TRES level of 0.22 ppb s<sup>-1</sup>. The modelled O<sub>3</sub>  
343 concentrations by the ‘one-box’ model largely underestimate the ‘true’ values, indicated by  
344 the negative  $\phi_{O_3}$  (within Region I), with small positive values for  $\phi_{O_3}$  only obtained at the  
345 lowest  $E_{NOx}$  (within Region II). The magnitude of  $\phi_{O_3}$  increases while  $E_{NOx}$  increases and the  
346 maximum level of  $\phi_{O_3}$  can be more than -30%. A large slope at the TRES for Case HE-H  
347 suggests that reductions in vehicle NO<sub>x</sub> emissions anticipated to arise from renewal of the  
348 vehicle fleet and implementation of more stringent emissions reduction technologies, will  
349 lead to a reduction in the magnitude of  $\phi_{O_3}$ , i.e. an improvement in model performance  
350 overall.

351

352 Figure 5(c) shows the results of  $\phi_{O_3}$  along the dot-dash line of Figure 4(f), i.e. varying  $E_{VOCs}$   
353 and  $E_{NOx}$  with the same emission ratio (i.e. 0.786) for the TRES (e.g. less or more trafficked  
354 areas). It is noted that the performance of the ‘one-box’ model for a less trafficked  
355 area/scenario (e.g. Birmingham) is better than that for a more trafficked area/scenario (e.g.  
356 London). Figure 5(c) also shows that the effect of  $w_t$  on  $\phi_{O_3}$  is relatively small for all cases.

However it is worth mentioning some secondary features that are counter intuitive, and thus not easily interpreted. Firstly, there exists a threshold of  $(E_{NOx}, E_{VOCs})$  below which, and another threshold of  $(E_{NOx}, E_{VOCs})$  above which,  $\phi_{O_3}$  for Case EX-L and  $\phi_{O_3}$  for Case EX-H are on the opposing sides of  $\phi_{O_3}$  for the base case; the first threshold of  $(E_{NOx}, E_{VOCs})$  is about  $6 \times (0.028, 0.022) \text{ ppb s}^{-1}$  and the second threshold of  $(E_{NOx}, E_{VOCs})$  is about  $10 \times (0.028, 0.022) \text{ ppb s}^{-1}$ . Between the two thresholds, the values of  $\phi_{O_3}$  for both Case EX-L and Case EX-H are larger than that for the case BASE. Secondly, according to intuition and linear reasoning, a higher  $w_t$  (Case EX-H) implies a better ventilation of the two street canyons with the background and in consequence a smaller difference between the two canyons; this effect would be similar to a smaller  $\varepsilon$  (Case HE-L) that implies a smaller difference between the two canyons. Therefore the points for Case EX-H (■) and Case HE-L (△) should appear on the same side of Case BASE (○); likewise the points for Case EX-L (▲) and Case HE-H (□) should appear on the same side of Case BASE (○). However, the results for  $O_3$  concentration in Figure 3 do not always support the reasoning, neither do the results for  $\phi_{O_3}$  in Figure 5. These all indicate the complexity of the nonlinear chemical system and suggest the necessity of in-depth analysis for specific scenarios.

Figure 5(d) shows the results of  $\phi_{O_3}$  along the trajectory from the year of 2005 to 2020 as indicated by Figure 4(f). It is noted that the level of extent of underestimation decreases with year, which indicates that in the future the performance of the ‘one-box’ model will be better. The underestimates of  $O_3$  concentration by the ‘one-box’ model for the year 2020 are -3.91% for Case BASE, -1.41% for Case HE-L, -7.60% for Case HE-H, -2.27% for Case EX-L and -3.47% for Case EX-H, respectively.

### 3.2 Intensity of segregation between $O_3$ and NO

Figure 6 illustrates the results of  $I_{S(O_3+NO)}$ , the intensity of segregation between  $O_3$  and NO, for all cases listed in Table 1 at the quasi-steady state ( $t=4 \text{ hr}$ ) as a function of  $E_{NOx}$  and  $E_{VOCs}$ . It is interesting to notice that the RSL (defined above) of each case divides the plot area into two regions, i.e. Region I where  $I_{S(O_3+NO)}$  is negative and Region II where  $I_{S(O_3+NO)}$  is positive as indicated in Figure 6(a)-(e). The trajectory from the year of 2005 to 2020 falls into

the negative region (i.e. Region I), and is marked in the plot for each case. It can be shown that the range of  $I_{S(O_3+NO)}$  (listed in Table 2) increases rapidly while  $\varepsilon$  increases from 0.3 to 0.7, i.e. (-7.78 %, 1.79 %) for Case HE-L, (-21.29 %, 5.21 %) for Case BASE and (-40.98 %, 11.02%) for Case HE-H. The range of  $I_{S(O_3+NO)}$  does not change significantly with the change of the exchange velocity from  $0.012 \text{ m s}^{-1}$  to  $0.028 \text{ m s}^{-1}$ , i.e. (-21.12 %, 6.78 %) for Case EX-L, (-21.29 %, 5.21 %) for Case BASE and (-21.18 %, 3.57) for Case EX-H. It is noted that the plots of  $I_{S(O_3+NO)}$  (Figure 6) are strongly correlated with those of  $\phi_{O_3}$  (Figure 4). In Region I for each case, the heterogeneity of emissions will lead to negative values of  $I_{S(O_3+NO)}$ , which means that the effective rate constant of the titration reaction ( $\text{NO} + \text{O}_3 \rightarrow \text{NO}_2 + \text{O}_2$ ) to consume  $\text{O}_3$ ,  $\langle k_{\text{eff}(O_3+NO)} \rangle = k_{(O_3+NO)}(1 + I_{S(O_3+NO)})$ , in the ‘two-box’ model is lower than the original rate constant,  $k_{(O_3+NO)}$ , in the ‘one-box’ model. In other words, adopting the classical rate constant  $k_{(O_3+NO)}$  in the ‘one-box’ model results in too much titration. As a result, the ozone level in the ‘two-box’ model (i.e. the ‘true’ value) is higher than the modelled ozone level from the ‘one-box’ model, which agrees well with a negative value of  $\phi_{O_3}$ , i.e. the modelled ozone level from the ‘one-box’ model is underestimated. In Region II for each case, a positive value of  $I_{S(O_3+NO)}$  is observed, which indicates that  $\langle k_{\text{eff}(O_3+NO)} \rangle$  is larger than  $k_{(O_3+NO)}$  and the ‘true’ value of  $\text{O}_3$  is less than the modelled value of  $\text{O}_3$  by the ‘one-box’ model. Therefore, a positive value of  $\phi_{O_3}$  is also observed in Region II, although the maximum overestimation only reaches 3.07 % (Table 2) for those scenarios considered here. Our findings also indicate that the slope of the RSL is determined by  $w_t$  (discussed above), while the pattern and range of  $\phi_{O_3}$  and  $I_{S(O_3+NO)}$  in Region I and Region II depend more closely on  $\varepsilon$ . It is also interesting to note that increasing  $\varepsilon$  will enhance the effect of segregation and therefore promote sub-grid scale variability and potentially systematic error in modelled  $\text{O}_3$  abundance. It appears that the impact of change in  $\varepsilon$  and  $w_t$  on  $\phi_{O_3}$  and  $I_{S(O_3+NO)}$  is nonlinear to  $E_{\text{NOx}}$  and  $E_{\text{VOCs}}$  due to the fact that  $\text{O}_3$  is a secondary, rather than the primary, pollutant.



Figure 7 shows the cross-sectional analyses, as indicated in Figure 6(f), of  $I_{S(O_3+NO)}$  (%). For the TRES emission scenario for the year of 2010 indicated by the solid line in Figure 7, the values of  $I_{S(O_3+NO)}$  are -15.47% for Case BASE, -5.38% for Case HE-L, -31.34% for Case HE-H, -9.93% for Case EX-L and -17.37% for Case EX-H, respectively. It is noted that at the fixed  $NO_x$  emission (Figure 7(a)), the magnitude of  $I_{S(O_3+NO)}$  for all cases decreases (becomes more negative) with reduced  $E_{VOCs}$ . However, at the fixed  $E_{VOCs}$  (Figure 7(b)), the value of  $I_{S(O_3+NO)}$  for each case decreases from positive to exclusively negative values with increased  $E_{NOx}$  in Region II and then becomes increasingly negative as  $E_{NOx}$  continues to increase in Region I. It is interesting that the smaller the values of  $\varepsilon$  or  $w_t$  (Figure 7(a) and Figure 7(b)) are, the smaller the magnitude of  $I_{S(O_3+NO)}$  (compared with Case BASE) will be. It can be seen from Figure 7(c) that  $I_{S(O_3+NO)}$  becomes less negative for less trafficked area/scenario and seems to be stable for the more polluted area/scenario. Figure 5(d) shows that the magnitudes of  $I_{S(O_3+NO)}$  decrease with year, suggesting that in the future the segregation effect on ozone levels would be less significant. The comparison between the plots in Figure 7 with their equivalents in Figure 5 also indicates a strong relationship between  $I_{S(O_3+NO)}$  and  $\phi_{O_3}$ .

#### 4 Conclusions

Segregation effects of heterogeneous emissions have been examined by considering the surface sub-grid emission heterogeneity in two idealised urban street canyons within the urban canopy layer and investigated how differing chemical effects (arising from the heterogeneity of emissions) and dynamic effects (i.e. exchange velocity) influence the error in  $O_3$  if implementing the grid-averaging parameterization for heterogeneous emissions. This study offers a better understanding of the parameterization of raw emissions for urban air quality models by highlighting the importance of segregation effects of heterogeneous emissions within the typical city-blocks (i.e. urban street canyons) and by providing a 2D pattern of overestimation for  $O_3$ . The common situations in urban areas are found to fall into Region I where the modelled  $O_3$  concentration in street canyons (lower than that in the overlying background atmosphere) by the ‘one-box’ model will be underestimated compared with the ‘true’ value by the ‘two-box’ model. Our findings also indicate that the performance of the ‘one-box’ model for  $O_3$  concentration is better for a more ‘green’ area with extra VOCs

sources and for the less trafficked area/scenario. Future emission trends are expected to lead to the error in the ‘one-box’ model approach falling. The error in ozone levels is strongly linked to segregation effects of heterogeneous emissions and is balanced by both dynamics and chemistry. This study is restricted to two boxes by considering only two typical street canyons with emission heterogeneity, which are totally segregated, neither transported nor mixed with each other. Future studies should take more photochemical boxes into consideration and model more scenarios well represented by more street canyons. Our final remark is that finding an appropriate real-world dataset to evaluate the box-averaged concentrations of this study is challenging due to the fact that concentrations of chemical species such as ozone are non-uniform inside a street canyon (Bright et al., 2013). Therefore high spatial density observations of pollutant concentrations inside street canyons are needed in support of a rigorous evaluation of the modelling approach. Recent development of low-cost sensors (e.g. Mead et al. 2013) provides a potential for the task to be completed in the future.

## **Acknowledgements**

The authors would like to thank Dr Vivien Bright for provision of the reduced chemical scheme (RCS). JZ thanks to the University of Birmingham for the award of a Li Siguang Scholarship, which is offered in partnership with the China Scholarship Council (CSC). The helpful comments of the anonymous reviewers are gratefully acknowledged.

467

468 Table 1. Overview of the model scenarios

Case	Heterogeneity of emissions ( $\epsilon$ )	Exchange velocity $w_t$ (m.s <sup>-1</sup> )
BASE	0.5	0.02
HE-L	0.3	0.02
HE-H	0.7	0.02
EX-L	0.5	0.012
EX-H	0.5	0.028

Note: 'BASE' is the base case. 'HE' denotes the heterogeneity of emissions, while 'EX' means the exchange velocity. 'L' or 'H' represents a lower or higher value than the corresponding component in the base Case BASE.

469

470

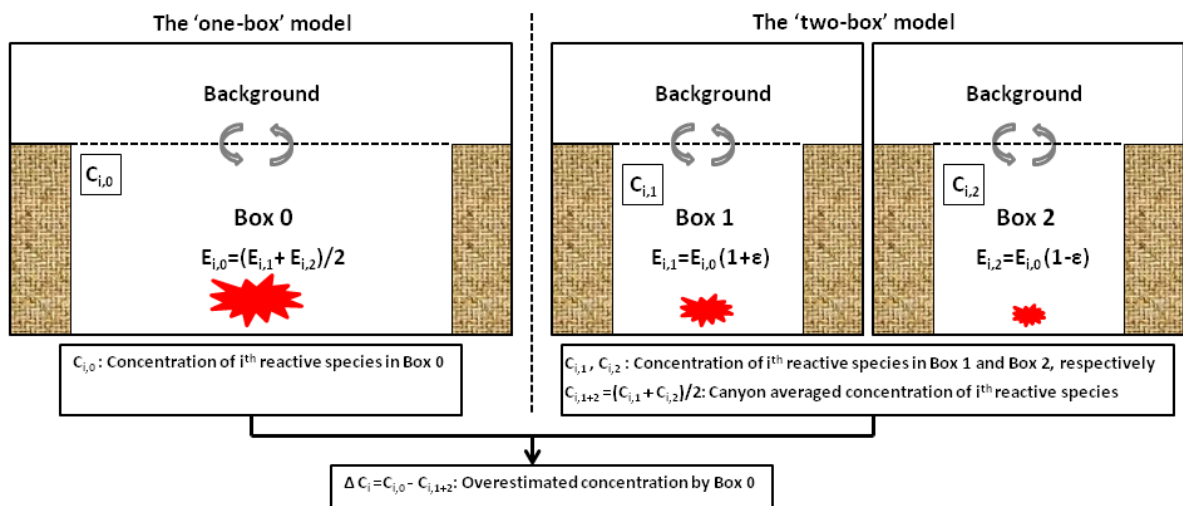
471 Table 2. Overview of the range of values among emission scenarios for all cases

Case	$C_{O_3,1+2}$ (ppb) (min, max)	$\phi_{O_3}$ (%) (min, max)	$I_{S(O_3+NO)}$ (%) (min, max)	Slope of RSL ( $E_{VOCs}$ ; $E_{NOx}$ )
BASE ( $\varepsilon=0.5$ , $w_f=0.02$ m s <sup>-1</sup> )	(7.56, 88.51)	(-17.35, 1.48)	(-21.29, 5.21)	2.6
HE-L ( $\varepsilon=0.3$ , $w_f=0.02$ m s <sup>-1</sup> )	(6.70, 89.16)	(-6.12, 0.52)	(-7.78, 1.79)	2.6
HE-H ( $\varepsilon=0.7$ , $w_f=0.02$ m s <sup>-1</sup> )	(9.69, 87.34)	(-35.24, 3.07)	(-40.98, 11.02)	2.6
EX-L ( $\varepsilon=0.5$ , $w_f=0.012$ m s <sup>-1</sup> )	(5.62, 160.82)	(-17.31, 2.26)	(-21.12, 6.78)	1.9
EX-H ( $\varepsilon=0.5$ , $w_f=0.028$ m s <sup>-1</sup> )	(9.58, 68.13)	(-17.25, 0.82)	(-21.18, 3.57)	3.4

Note: 'BASE' is the base case. 'HE' denotes the heterogeneity of emissions, while 'EX' means the exchange velocity. 'L' or 'H' represents a lower or higher value than the corresponding component in the base Case BASE.  $C_{O_3,1+2}$  denotes the true concentration of  $O_3$  (ppb);  $\phi_{O_3}$  means the *percentage of overestimation* for  $O_3$  by the 'one-box' model (%);  $I_{S(O_3+NO)}$  is the *intensity of segregation* between  $O_3$  and NO (%); RSL represents the Region Split Line;  $E_{VOCs}$  and  $E_{NOx}$  are the emission rates of VOCs and  $NO_x$ , respectively (ppb s<sup>-1</sup>).

472

473



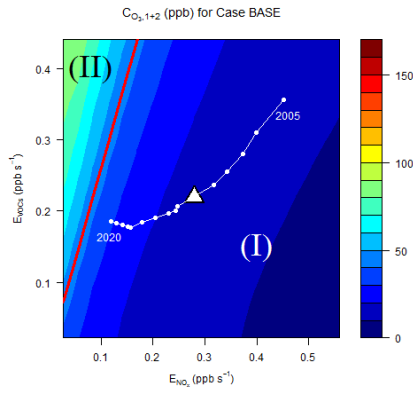
474

475 Figure 1. Overview of the model setup.  $E_{i,m}$  means the emission rate of  $i^{\text{th}}$  species in Box  $m$  ( $m=0,1,2$ ) ( $\text{ppb s}^{-1}$ );

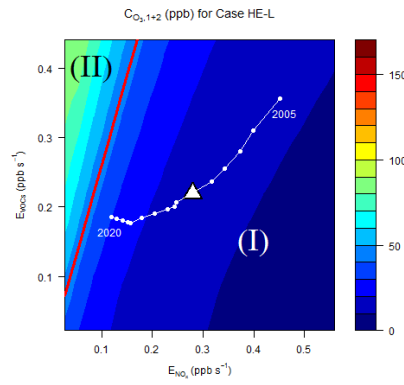
476  $\varepsilon$  is the heterogeneity of emissions.

477

(a)



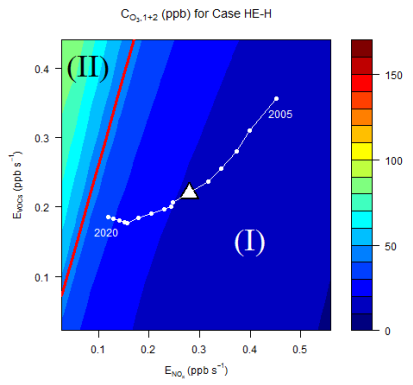
(b)



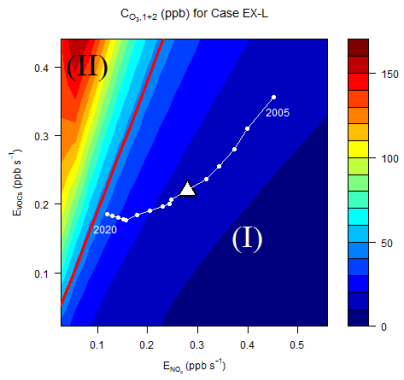
478

479

(c)



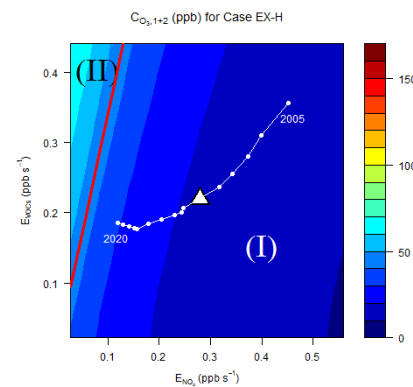
(d)



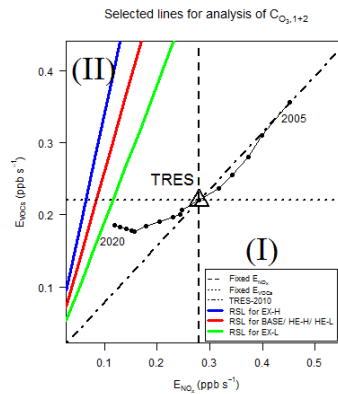
480

481

(e)



(f)



482

483

484

485

486

487

Figure 2.  $C_{O_3,1+2}$  (ppb), the ‘true’ concentration of  $O_3$  derived from the ‘two-box’ model, in the (a) Case BASE, (b) Case HE-L, (c) Case HE-H, (d) Case EX-L, (e) Case EX-H and (f) Selected lines for analysis.  $E_{VOCs}$  and  $E_{NOx}$  are the emission rates of VOCs and  $NO_x$ , respectively ( $ppb\ s^{-1}$ ); RSL means Region Split Line;  $\triangle$  represents the ‘Typical Real-world Emission Scenario’, TRES, for the year of 2010; The trajectory from 2005 to 2020 represents the emission scenarios for 2005 to 2020, assuming constant traffic volume and speed.

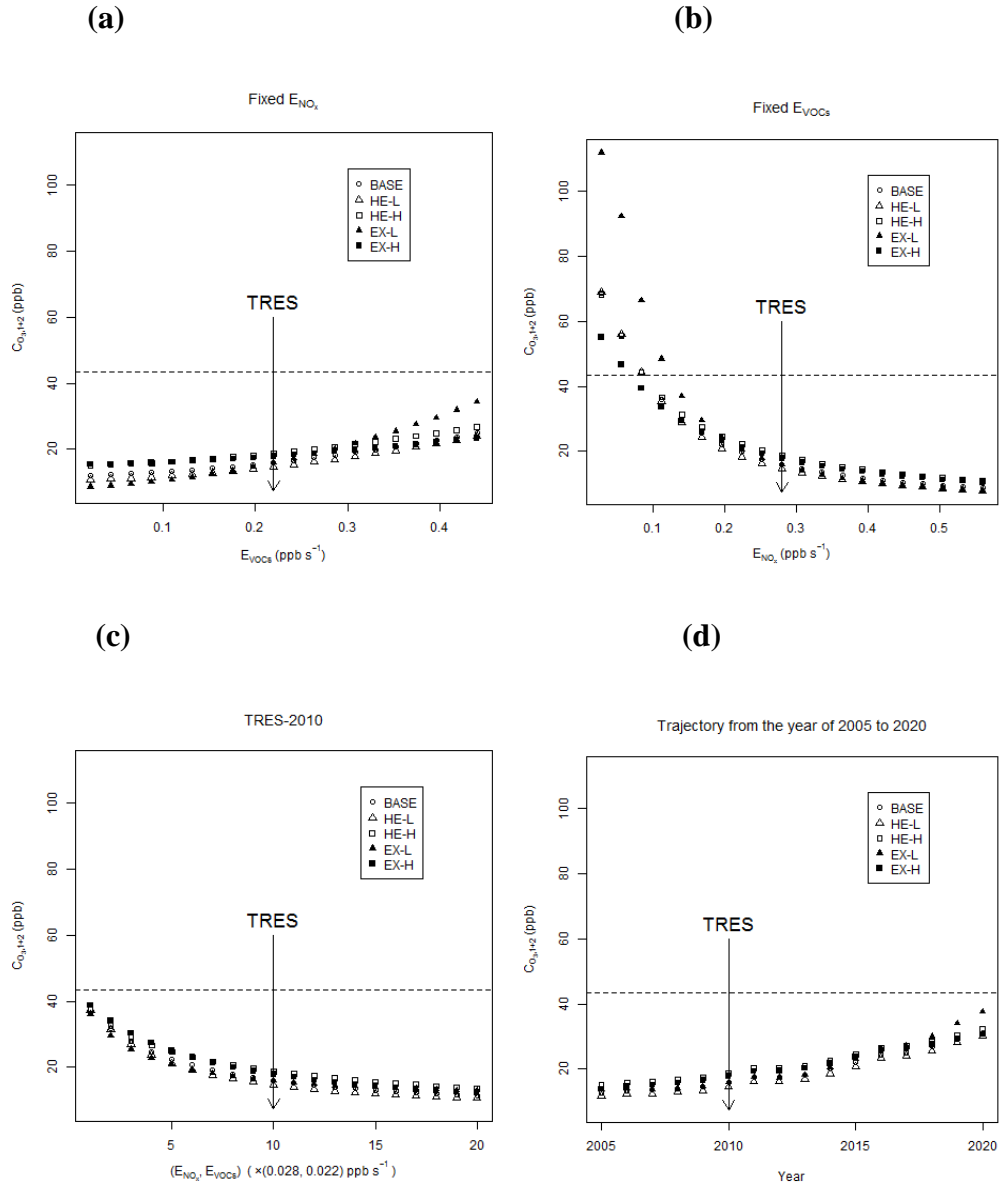


Figure 3.  $C_{O_3,1+2}$  (ppb), the ‘true’ concentration of  $O_3$  derived from the ‘two-box’ model, for (a) “Fixed  $E_{NO_x}$ ” at a fixed  $NO_x$  emissions ( $0.28 \text{ ppb s}^{-1}$ ), (b) “Fixed  $E_{VOCs}$ ” at a fixed  $VOCs$  emissions ( $0.22 \text{ ppb s}^{-1}$ ), (c) “TRES-2010” varying the total traffic volume only and (d) “Trajectory from the year of 2005 to 2020” assuming constant traffic volume and speed.  $E_{VOCs}$  and  $E_{NO_x}$  are the emission rates of  $VOCs$  and  $NO_x$ , respectively ( $\text{ppb s}^{-1}$ ); The dashed line indicates the background  $O_3$  level of  $43.61 \text{ ppb}$ ; The solid line indicates the ‘Typical Real-world Emission Scenario’, TRES, for the year of 2010.

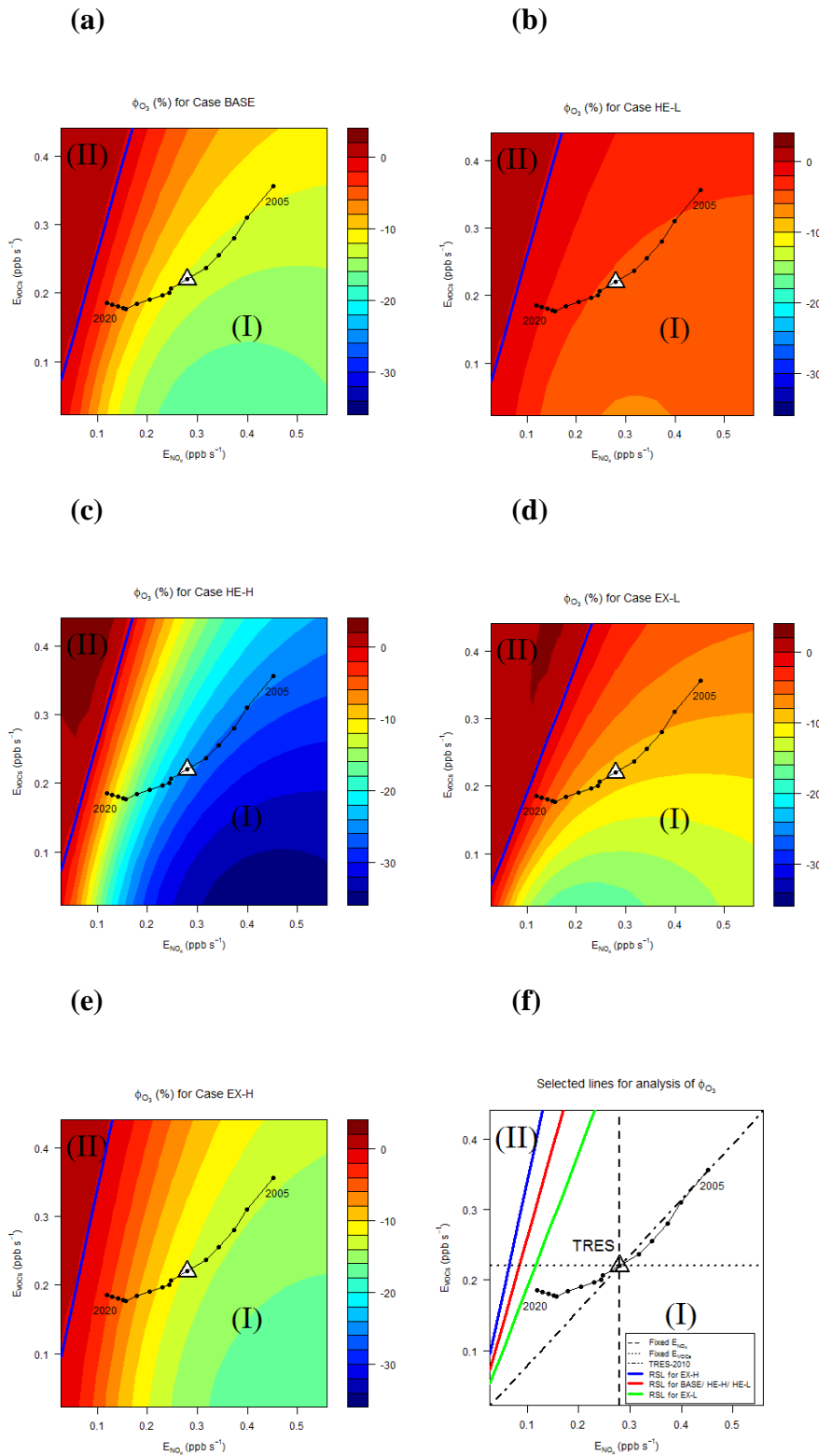


Figure 4.  $\phi_{O_3}$  (%), the percentage of overestimation for  $O_3$  by the ‘one-box’ model, in the (a) Case BASE, (b) Case HE-L, (c) Case HE-H, (d) Case EX-L, (e) Case EX-H and (f) Selected lines for analysis.  $E_{VOCs}$  and  $E_{NOx}$  are the emission rates of VOCs and  $NO_x$ , respectively (ppb s<sup>-1</sup>); RSL means Region Split Line;  $\triangle$  represents the ‘Typical Real-world Emission Scenario’, TRES, for the year of 2010; The trajectory from 2005 to 2020 means the emission scenarios for 2005 to 2020, assuming constant traffic volume and speed.



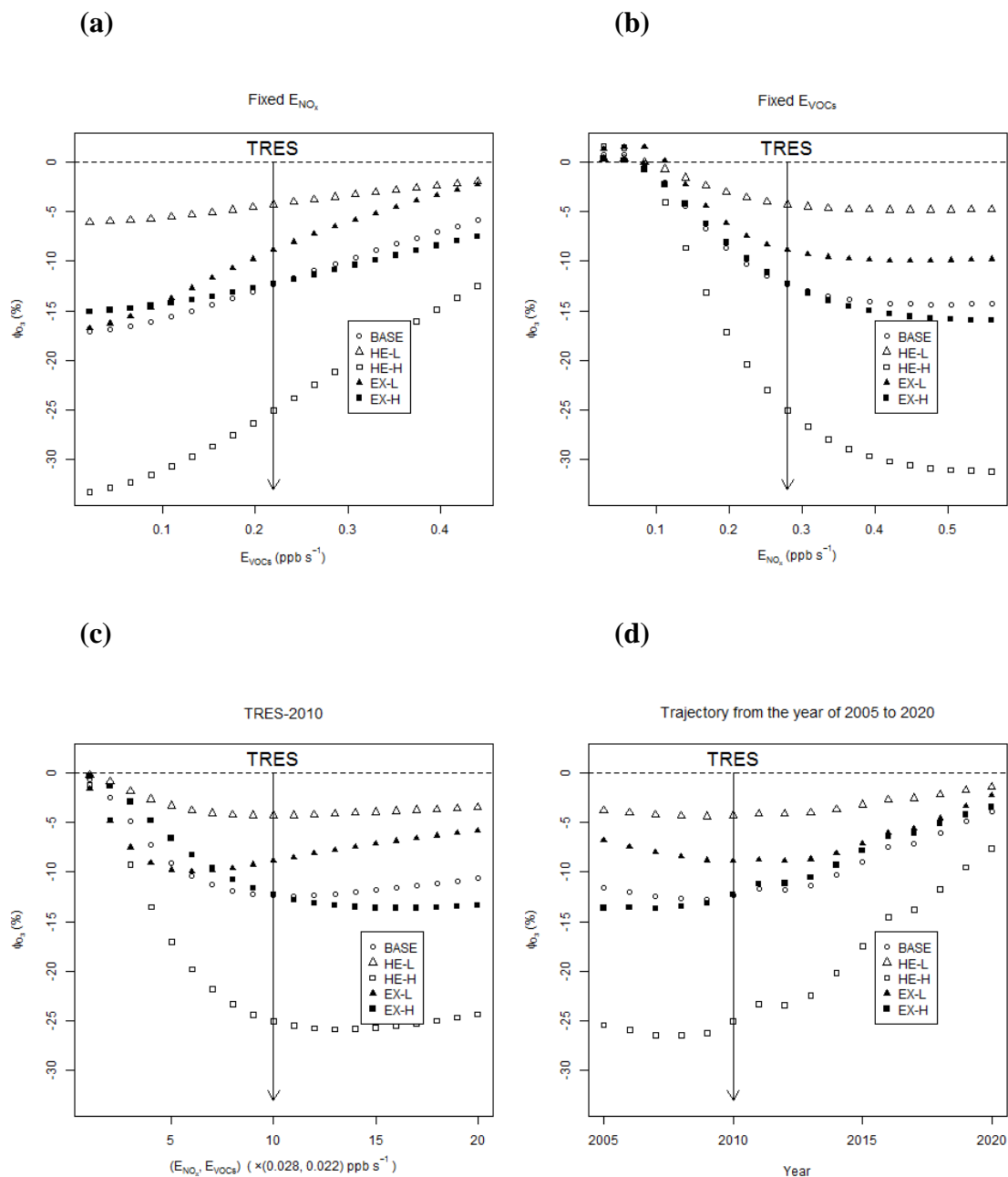
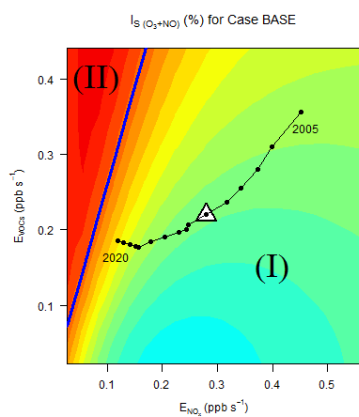


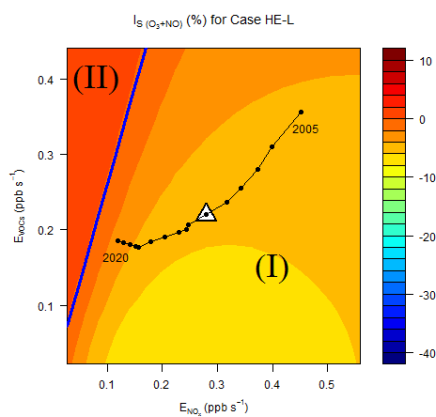
Figure 5.  $\phi_{O_3}$  (%), the percentage of overestimation for  $O_3$  by the ‘one-box’ model, for (a) “Fixed  $E_{NO_x}$ ” at a fixed  $NO_x$  emissions ( $0.28 \text{ ppb s}^{-1}$ ), (b) “Fixed  $E_{VOCs}$ ” at a fixed VOCs emissions ( $0.22 \text{ ppb s}^{-1}$ ), (c) “TRES-2010” varying the total traffic volume only and (d) “Trajectory from the year of 2005 to 2020” assuming constant traffic volume and speed.  $E_{VOCs}$  and  $E_{NO_x}$  are the emission rates of VOCs and  $NO_x$ , respectively ( $\text{ppb s}^{-1}$ ); The solid line indicates the ‘Typical Real-world Emission Scenario’, TRES, for the year of 2010.

523

(a)



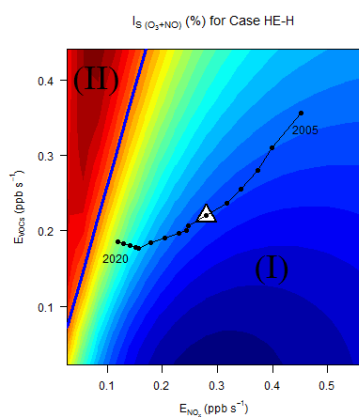
(b)



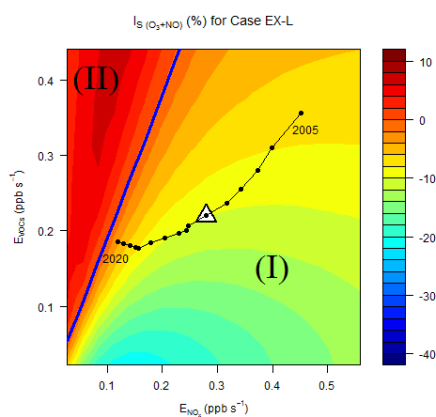
524

525

(c)



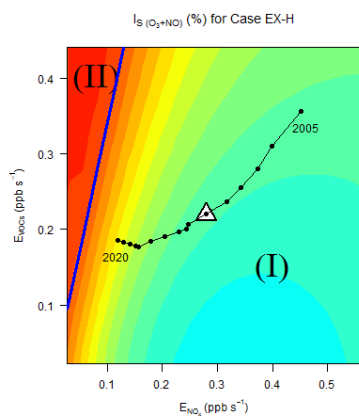
(d)



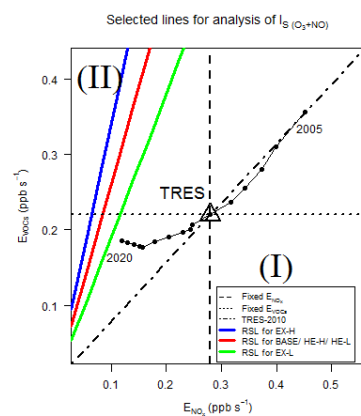
526

527

(e)



(f)



528

529

530

531

Figure 6.  $I_{S(O_3+NO)}$  (%), the intensity of segregation between  $O_3$  and  $NO$ , in the (a) Case BASE, (b) Case HE-L, (c) Case HE-H, (d) Case EX-L, (e) Case EX-H and (f) Selected lines for analysis.  $E_{VOCs}$  and  $E_{NOx}$  are the emission rates of VOCs and  $NO_x$ , respectively ( $ppb\ s^{-1}$ ); RSL means Region Split Line;  $\triangle$  represents the 'Typical

Real-world Emission Scenario', TRES, for the year of 2010; The trajectory from 2005 to 2020 indicates the emission scenarios for 2005 to 2020, assuming constant traffic volume and speed.

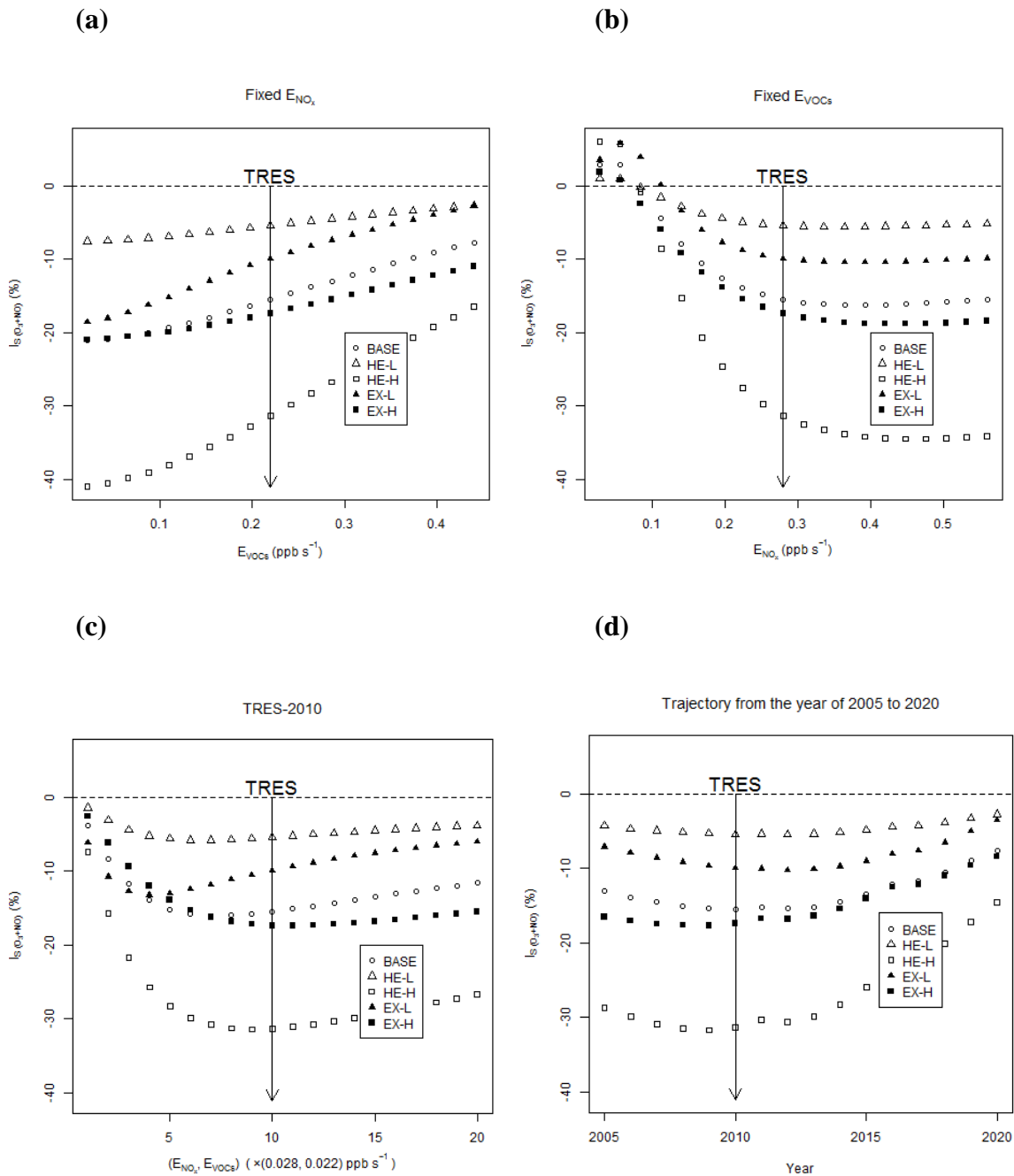


Figure 7.  $I_{S(O_3+NO)}$  (%), the intensity of segregation between  $O_3$  and  $NO$ , for (a) “Fixed  $E_{NOx}$ ” at a fixed  $NO_x$  emissions ( $0.28 \text{ ppb s}^{-1}$ ), (b) “Fixed  $E_{VOCs}$ ” at a fixed  $VOCs$  emissions ( $0.22 \text{ ppb s}^{-1}$ ), (c) “TRES-2010” varying the total traffic volume only and (d) “Trajectory from the year of 2005 to 2020” assuming constant traffic volume and speed.  $E_{VOCs}$  and  $E_{NOx}$  are the emission rates of  $VOCs$  and  $NO_x$ , respectively ( $\text{ppb s}^{-1}$ ); The solid line indicates the ‘Typical Real-world Emission Scenario’, TRES, for the year of 2010.

## 544 **References**

- 545 Arciszewska, C. and McClatchey, J.: The importance of meteorological data for modelling air  
546 pollution using ADMS-Urban. *Meteorological Applications*, 8, 345-350, 2001.
- 547 Auger, L. and Legras, B.: Chemical segregation by heterogeneous emissions. *Atmospheric*  
548 *Environment*, 41, 2303-2318, 2007.
- 549 Beevers, S. D., Kitwiroon, N., Williams, M. L. and Carslaw, D. C.: One way coupling of  
550 CMAQ and a road source dispersion model for fine scale air pollution predictions.  
551 *Atmospheric Environment*, 59, 47-58, 2012.
- 552 Boulter, P. G., Barlow, T. J., Latham, S. and McCrae, I. S.: Emission Factors 2009: Report 1  
553 - a review of methods for determining hot exhaust emission factors for road vehicles.  
554 TRL: Wokingham, 2009.
- 555 Bright, V. B., Bloss, W. J. and Cai, X. M.: Urban street canyons: Coupling dynamics,  
556 chemistry and within-canyon chemical processing of emissions. *Atmospheric*  
557 *Environment*, 68, 127-142, 2013.
- 558 Cai, X.-M.: Effects of differential wall heating in street canyons on dispersion and ventilation  
559 characteristics of a passive scalar. *Atmospheric Environment*, 51, 268-277, 2012.
- 560 Cassiani, M., Vinuesa, J. F., Galmarini, S. and Denby, B.: Stochastic fields method for sub-  
561 grid scale emission heterogeneity in mesoscale atmospheric dispersion models.  
562 *Atmospheric Chemistry and Physics*, 10, 267-277, 2010.
- 563 Chemel, C., Sokhi, R. S., Dore, A. J., Sutton, P., Vincent, K. J., Griffiths, S. J., Hayman, G.  
564 D., Wright, R. D., Baggaley, M., Hallsworth, S., Prain, H. D. and Fisher, B. E. A.:  
565 Predictions of UK Regulated Power Station Contributions to Regional Air Pollution  
566 and Deposition: A Model Comparison Exercise. *Journal of the Air & Waste*  
567 *Management Association*, 61, 1236-1245, 2011.
- 568 Ching, J., Herwehe, J. and Swall, J.: On joint deterministic grid modeling and sub-grid  
569 variability conceptual framework for model evaluation. *Atmospheric Environment*,  
570 40, 4935-4945, 2006.
- 571 Chung, T. N. H. and Liu, C.-H.: On the Mechanism of Air Pollutant Removal in Two-  
572 Dimensional Idealized Street Canyons: A Large-Eddy Simulation Approach.  
573 *Boundary-Layer Meteorology*, 148, 241-253, 2013.
- 574 Curtis, A. R. and Sweetenham, W. P.: FACSIMILE/CHECKMAT user's manual. UKAEA  
575 Atomic Energy Research Establishment Computer Science and Systems Division,  
576 1987.
- 577 Constantinescu, E. M., Sandu, A. and Carmichael, G. R.: Modeling atmospheric chemistry  
578 and transport with dynamic adaptive resolution. *Computational Geosciences*, 12, 133-  
579 151, 2008.
- 580 Denby, B., Cassiani, M., de Smet, P., de Leeuw, F. and Horalek, J.: Sub-grid variability and  
581 its impact on European wide air quality exposure assessment. *Atmospheric*  
582 *Environment*, 45, 4220-4229, 2011.
- 583 Fisher, B., Kukkonen, J., Piringer, M., Rotach, M. W. and Schatzmann, M.: Meteorology  
584 applied to urban air pollution problems: concepts from COST 715. *Atmospheric*  
585 *Chemistry and Physics*, 6, 555-564, 2006.

Galmarini, S., Vinuesa, J. F. and Martilli, A.: Modeling the impact of sub-grid scale emission variability on upper-air concentration. *Atmospheric Chemistry and Physics*, 8, 141-158, 2008.

Garcia-Menendez, F. and Odman, M. T.: Adaptive Grid Use in Air Quality Modeling. *Atmosphere*, 2, 484-509, 2011.

Garcia-Menendez, F., Yano, A., Hu, Y. T. and Odman, M. T.: An adaptive grid version of CMAQ for improving the resolution of plumes. *Atmospheric Pollution Research*, 1, 239-249, 2010.

Grell, G. A., Peckham, S. E., Schmitz, R., McKeen, S. A., Frost, G., Skamarock, W. C. and Eder, B.: Fully coupled "online" chemistry within the WRF model. *Atmospheric Environment*, 39, 6957-6975, 2005.

Hilst, G. R.: Segregation and chemical reaction rates in air quality models. *Atmospheric Environment*, 32, 3891-3895, 1998.

Isakov, V., Touma, J. S., Burke, J., Lobdell, D. T., Palma, T., Rosenbaum, A. and Ozkaynak, H.: Combining Regional- and Local-Scale Air Quality Models with Exposure Models for Use in Environmental Health Studies. *Journal of the Air & Waste Management Association*, 59, 461-472, 2009.

Johnson, M., Isakov, V., Touma, J. S., Mukerjee, S. and Ozkaynak, H.: Evaluation of land-use regression models used to predict air quality concentrations in an urban area. *Atmospheric Environment*, 44, 3660-3668, 2010.

Karamchandani, P., Seigneur, C., Vijayaraghavan, K. and Wu, S. Y.: Development and application of a state-of-the-science plume-in-grid model. *Journal of Geophysical Research-Atmospheres*, 107, 2002.

Karamchandani, P., Vijayaraghavan, K. and Yarwood, G.: Sub-Grid Scale Plume Modeling. *Atmosphere*, 2, 389-406, 2011.

Karamchandani, P., Zhang, Y. and Chen, S. Y.: Development and initial application of a sub-grid scale plume treatment in a state-of-the-art online Multi-scale Air Quality and Weather Prediction Model. *Atmospheric Environment*, 63, 125-134, 2012.

Kesarkar, A. P., Dalvi, M., Kaginalkar, A. and Ojha, A.: Coupling of the Weather Research and Forecasting Model with AERMOD for pollutant dispersion modeling. A case study for PM10 dispersion over Pune, India. *Atmospheric Environment*, 41, 1976-1988, 2007.

Krol, M. C., Molemaker, M. J. and de Arellano, J. V. G.: Effects of turbulence and heterogeneous emissions on photochemically active species in the convective boundary layer. *Journal of Geophysical Research-Atmospheres*, 105, 6871-6884, 2000.

Lee, J. D., Lewis, A. C., Monks, P. S., Jacob, M., Hamilton, J. F., Hopkins, J. R., Watson, N. M., Saxton, J. E., Ennis, C., Carpenter, L. J., Carslaw, N., Fleming, Z., Bandy, B. J., Oram, D. E., Penkett, S. A., Slemr, J., Norton, E., Rickard, A. R., Whalley, L. K., Heard, D. E., Bloss, W. J., Gravestock, T., Smith, S. C., Stanton, J., Pilling, M. J. and Jenkin, M. E.: Ozone photochemistry and elevated isoprene during the UK heatwave of August 2003. *Atmospheric Environment*, 40, 7598-7613, 2006.

628 Liu, C.-H. and Leung, D. Y. C.: Numerical study on the ozone formation inside street  
629 canyons using a chemistry box model. *Journal of Environmental Sciences-China*, 20,  
630 832-837, 2008.

631 Loughner, C. P., Allen, D. J., Zhang, D.-L., Pickering, K. E., Dickerson, R. R. and Landry,  
632 L.: Roles of Urban Tree Canopy and Buildings in Urban Heat Island Effects:  
633 Parameterization and Preliminary Results. *Journal of Applied Meteorology and*  
634 *Climatology*, 51, 1775-1793, 2012.

635 Mead, M.I., Popoola, O.A.M., Stewart, G.B., Landshoff, P., Calleja, M., Hayes, M., Baldovi,  
636 J.J., McLeod, M.W., Hodgson, T.F., Dicks, J., Lewis, A., Cohen, J., Baron, R.,  
637 Saffell, J.R., Jones, R.L.,. The use of electrochemical sensors for monitoring urban air  
638 quality in low-cost, high-density networks. *Atmospheric Environment* 70, 186-203,  
639 2013.

640 NAEI: UK fleet composition projections. URL: <http://naei.defra.gov.uk/data/ef-transport>,  
641 2003.

642 Shen, J., Wang, X. S., Li, J. F., Li, Y. P. and Zhang, Y. H.: Evaluation and intercomparison  
643 of ozone simulations by Models-3/CMAQ and CAMx over the Pearl River Delta.  
644 *Science China-Chemistry*, 54, 1789-1800, 2011.

645 Shrestha, K. L., Kondo, A., Kaga, A. and Inoue, Y.: High-resolution modeling and evaluation  
646 of ozone air quality of Osaka using MM5-CMAQ system. *Journal of Environmental*  
647 *Sciences-China*, 21, 782-789, 2009.

648 Sokhi, R. S., San Jose, R., Kitwiroon, N., Fragkou, E., Perez, J. L. and Middleton, D. R.:  
649 Prediction of ozone levels in London using the MM5-CMAQ modelling system.  
650 *Environmental Modelling & Software*, 21, 566-576, 2006.

651 Srivastava, R. K., McRae, D. S. and Odman, M. T.: An adaptive grid algorithm for air-quality  
652 modeling. *Journal of Computational Physics*, 165, 437-472, 2000.

653 Stein, A. F., Isakov, V., Godowitch, J. and Draxler, R. R.: A hybrid modeling approach to  
654 resolve pollutant concentrations in an urban area. *Atmospheric Environment*, 41,  
655 9410-9426, 2007.

656 Stocker, J., Hood, C., Carruthers, D. and McHugh, C.: ADMS-Urban: developments in  
657 modelling dispersion from the city scale to the local scale. *International Journal of*  
658 *Environment and Pollution*, 50, 308-316, 2012.

659 Touma, J. S., Isakov, V., Ching, J. and Seigneur, C.: Air quality modeling of hazardous  
660 pollutants: Current status and future directions. *Journal of the Air & Waste*  
661 *Management Association*, 56, 547-558, 2006.

662 Vijayaraghavan, K., Karamchandani, P. and Seigneur, C.: Plume-in-grid modeling of summer  
663 air pollution in Central California. *Atmospheric Environment*, 40, 5097-5109, 2006.

664 Vinuesa, J. F. and de Arellano, J. V. G.: Introducing effective reaction rates to account for the  
665 inefficient mixing of the convective boundary layer. *Atmospheric Environment*, 39,  
666 445-461, 2005.

667 Zou, B., Zhan, F. B., Wilson, J. G. and Zeng, Y. N.: Performance of AERMOD at different  
668 time scales. *Simulation Modelling Practice and Theory*, 18, 612-623, 2010.